Heliyon 10 (2024) e38233

Contents lists available at ScienceDirect

Heliyon

journal homepage: www.cell.com/heliyon

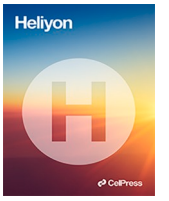

Research article

Experimental studies on the cooling and heating performance of a highly emissive coating

Zhuo Yang [a,b], Zhangran Yang [c], Zihan Zhang [d], Yuanzhu Cai [b], Xingjian Wang [e], Yanwen Li [b], Ruohan Zhang [f], Yangang Zhang [b], Lianhua Liu [b], Weidong Zhang [b,*], Lijin Xu [a,**], Peng Wang [a,***]

[a] School of Chemistry and Life Resources, Renmin University, Beijing, 100872, China
[b] China Southwest Architectural Design and Research Institute Co., Ltd., Chengdu, 610042, China
[c] School of Materials Science and Engineering, Shanghai Institute of Technology, Shanghai, 201418, China
[d] School of Network Engineering, Zhengzhou University of Economics and Business, Zhengzhou, 451191, China
[e] School of Chemistry and Chemical Engineering, Ningxia University, Yinchuan, 750021, China
[f] School of Foreign Languages, Capital Normal University, Beijing, 10089, China

ARTICLE INFO

Keywords:
Highly emissive coating
Solar reflectance
Emissivity
Heat dissipation
Heating energy efficiency

ABSTRACT

In this study, the cooling effect below ambient air temperature, heat dissipation properties and heating energy efficacy of a superomniphobic self-cleaning (SSC) highly emissive (HE) coating were systematically investigated. Except at midday, the SSC-HE coating with an extremely high solar reflectance of 0.985 showed a better cooling effect than a 10-cm-thick polyurethane insulation layer. The coating substantially reduced the interior air temperature of a well-insulated system by as much as 6.9 °C. The SSC-HE coating enabled the roof surface and room temperatures of the brick bungalow to be 3.4 and 10.2 °C below the ambient air temperature, respectively. Compared with the sunshade and spray water, the SSC-HE coating exhibited better cooling effect. The SSC topcoat allowed the battery cabinet of an HE-coated distributed telecommunication base station to remain its original sub-ambient cooling effect for a long time. Regardless of the location of the HE-coated metal facility, the ultrahigh emissivity of the coating enabled it to exhibit excellent heat dissipation performance during both day and night, even under adiabatic conditions. Additionally, under identical room temperature settings, the HE-coated electric oil heater not only showed faster heating but also had heating energy efficiency of 5.9 % and 4.4 % relative to heaters coated with aluminium- and black paints, respectively. Under identical heating power consumption levels, compared to black paint-coated heater, the HE-coated heater endowed the surrounding environment with a higher equilibrium air temperature, improving the thermal comfort of the indoor environment.

* Corresponding author.
** Corresponding author.
*** Corresponding author.
E-mail addresses: zwdpt@sohu.com (W. Zhang), 20050062@ruc.edu.cn (L. Xu), wpeng_chem@ruc.edu.cn (P. Wang).

https://doi.org/10.1016/j.heliyon.2024.e38233
Received 24 June 2024; Received in revised form 19 September 2024; Accepted 20 September 2024
Available online 21 September 2024

1. Introduction

To maintain the thermal comfort in the indoor environment, heating, ventilation and air conditioning (HVAC) systems consume more than 50 % of the residential energy consumption in the United States [1]. Among HVAC systems, cooling by air conditioning itself contributes to 15 % of building energy usages in the United States [2]. Unlike heating, peak cooling demand occurs during the daytime [2]. Therefore, sub-ambient radiative cooling (SDRC) has a significant impact on the global energy consumption.

The sub-ambient radiative cooling under direct sunlight was primarily achieved using titanium dioxide rutile (TiO_2) white paints [3] under ideal atmospheric conditions. However, because of the moderate 3.2 eV electron band gap of TiO_2, TiO_2-based white coatings have weak spectral reflectance in the ultraviolet (UV) region (250−400 nm) [4–6], which makes up 5 % of solar heat. In addition, the binder of coatings results in a strong absorption in the near infrared (NIR) region (700−2500 nm). Consequently, TiO_2 white paints cannot meet the stringent requirement that more than 94 % of sunlight must be reflected to achieve meaningful SDRC under any atmospheric condition [2].

To date, various materials have been employed to realise SDRC over a variety of substrates using different methods [2,7–31]. Among the SDRC technologies that have become scalable, paint coatings [3–6,13,18,20,21,24,26,30] are likely to be widely used, owing to their easy fabrication and adaptability to various substrates. Single-story concrete and carbon steel-based prefabricated buildings painted with a fluorescent daytime radiative cooling coating [32] and superomniphobic self-cleaning (SSC) SDRC coating [33,34] have exhibited significant sub-ambient cooling effects of 2.6–10.6 °C under direct sunlight, corresponding to a cooling energy efficiency of 27%–50.2 % relative to their cool-white-coated counterparts [34]. Without air conditioning, the thermal comfort of the living environment can be significantly improved using the SDRC coating during the summer.

SDRC coatings have also been widely applied for low-temperature grain and edible-oil storages. The wheat pile's interior temperature in a SSC-SDRC coated grain silo was reduced up to 10 °C compared to that in the control silo [35]. Moreover, the interior air temperature of a SDRC-coated edible oil storage tank was 38.3 °C lower than that of the control, thus greatly improving the storage safety.

To reduce the cooling electricity consumption of telecommunications base stations (TBSs), various distributed TBSs in different climatic regions of China were painted with the SSC-SDRC coating. Applying the SDRC coating reduced the interior air temperature of an equipment cabinet by 10.4 °C during the midday and by 6.0 °C at night, resulting in cooling energy efficacies from 31.7 % to 64.9 % [36]. In Panzhihua, SSC-SDRC-painted equipment cabinets reduced the cooling power consumption by as much as 2083.2 kWh in 290 d compared to the cool-white-coated counterpart [37].

In addition to the paint coatings, a silver-coated membrane was applied to large warehouses of wine [38] to result in cooling energy efficiency of 44.6 %. When the membrane was applied to grain storage warehouses [39], it decreased the interior air and grain temperatures by as much as 9.8 and 4.0 °C, respectively.

The above studies all focused on the radiative cooling effect below the ambient air temperature and cooling electricity conservation on uninsulated or normally-insulated structures. Moreover, regardless of these practical sub-ambient cooling results, the cooling effects of the SDRC coatings applied to other types of buildings, the comparison of the SDRC coating with other thermal management solutions and the long-term cooling performance of the SDRC coating are also of great importance and worthy of in-depth research. In addition, when applied to well-insulated structures such as a refrigerated warehouse, it is assumed that SDRC materials were not as much effective in cooling as the above substrates because thermal insulation minimizes the heat transfer through the enclosure structure. It is imperative to conduct relevant studies.

On the other hand, heating is also a significant end-use of energy globally. For example, the residential buildings in China and EU are responsible for approximately 24 % [40] and 26 % [41] of final energy consumption, respectively, and the heating energy usages account for 24.7 % and 64 % of this consumption, respectively. In practice, the infrared emissivity of a material must be sufficiently high to realise meaningful SDRC. The dissipate heat rate of a material is determined by its emissivity [42]. Hence, this raises the question of whether SDRC coatings can also be applied to equipment, heat sinks, condensers, and heaters for fast heat dissipation and heating energy efficacy in winter. However, to the best of our knowledge, to date there is no paper related to the application of the heat dissipation performance of SDRC materials.

To address these interesting scientific issues, we conducted a systematic investigation using a self-fabricated highly emissive (HE) coating with extremely high solar reflectance. When applied to structures exposed to the outdoor environment, a self-developed SSC topcoat was introduced as the topcoat to protect the HE coating from dirt accumulation. In this study, the solar reflectance, emissivity and thermal conductivity of the SSC-HE coating were characterised. Moreover, the SDRC effects of the SSC-HE coating on a well-insulated structure, a brick bungalow and a chemical pipeline were presented. The long-term cooling performance of the coating was highlighted. The heat dissipation rates of the HE coating and stainless steel container were compared. Additionally, improvements in thermal comfort and heating energy efficiency when applied to heaters were discussed.

2. Principles of SDRC and heat dissipation

For a surface exposed to a daylight sky, the following four thermal phenomena can be observed: the power P_{rad} emitted by the surface at the surface temperature T_s; the incident down welling atmospheric infrared radiation P_{atm} absorbed by the surface; the incident solar radiation P_{sun} absorbed by the surface; the incident heat from the ambient due to conduction and convection $P_{cond+conv}$. The radiative cooling power P_{cool} can be expressed in Eq. (1) as follows [2,9]:

$$P_{cool} = P_{rad} - P_{atm} - P_{sun} - P_{cond+conv} \quad (1)$$

The radiative cooling power can be further correlated with the emissivity ε, solar reflectance R of the surface, solar irradiation I, the absolute surface temperature T_s, the absolute effective sky temperature T_{sky}, and the absolute ambient air temperature T_{amb}, as shown in Eq. (2) [2]:

$$P_{cool} = \varepsilon\sigma\left(T_s^4 - T_{sky}^4\right) - (1-R)I - h_{cond+conv}(T_{amb} - T_s) \quad (2)$$

where σ and $h_{cond\ +\ conv}$ are the Stefan-Boltzmann constant (5.67×10^{-8} $Wm^{-2}K^{-1}$) and the conduction and convection heat coefficient, respectively.

When $P_{cool} = 0$, $T_s < T_{am}$ and the surface reaches a steady state below ambient air temperature. The solution of Eq. (2) yields the subambient equilibrium temperature T_s.

According to the Stefan–Boltzmann law, the radiative heat transfer rate of an object is directly proportional to its surface area (A) and P_{rad}, as follows:

$$Q = AP_{rad} = \varepsilon\sigma AT_s^4 \quad (3)$$

where Q is the radiation heat transfer rate (J/s). Therefore, the higher the emissivity of an object, the faster the heat dissipation rate, and the better the heat dissipation performance will be.

3. Experimental section

3.1. Description of the HE and SSC coatings

To investigate the cooling effects below ambient air temperature and heat dissipation performance on different substrates, we manufactured a HE coating, whose optimised composition was as follows: acrylate emulsion (16.6 wt%), water (6.3 wt%), wetting agent (0.2 wt%), dispersant (0.3 wt%), antifoaming agent (0.3 wt%), levelling agent (0.4 wt%), coalescent (0.3 wt%), barium sulphate (74.0 wt%), and calcium carbonate (1.6 wt%) [6].

In addition, the optimised composition of the transparent SSC topcoat was as follows: hydrophilic silica nanoparticles (0.25 wt%), tetraethoxysilane (TEO, 0.34 wt%), perfluorodecyltriethoxysilane (PFDTES, 0.51 wt%), absolute alcohol (85.2 wt%) and aqueous ammonia (13.7 wt%).

The manufacture processes to fabricate the HE and SSC coatings were described in a previous study [6]. For the SSC topcoat, the contact and sliding angles of water were 163.4°and 2°, respectively; the contact and sliding angles for n-hexadecane were 151.4° and 9°, respectively [6].

For the SSC topcoat, fluorinated polysiloxane (fluoro-POS) modification via hydrolysis and co-polycondensation formed a network structure composed of silicone-oxygen bonds and endowed the two-layer coating system with an extremely low surface free energy and high transparency [6]. Additionally, as shown by the scanning electron microscopy (SEM) images of the SSC-HE coating, the two-layer coating had a micro-nano hierarchical structure, which significantly increased the roughness of the coating surface [6].

The HE and SSC coatings were applied to different substrates. The dry coating thickness of the HE coating was no less than 400 μm and that of the SSC coating was no thicker than 50 μm.

3.2. Measurements of optical and thermal properties

Following ASTM E903-20 (standard test method for solar absorbance, reflectance, and transmittance of materials using integrating spheres), a UV/VIS/NIR spectrophotometer (Lambda 950) equipped with an integrating sphere (150 mm diameter, Labsphere RSA-PE-19) was used to measure the spectral reflectance of the PSDRC coating. The solar reflectance was calculated by integrating the measured spectral data weighted with the air mass of 1.5 beam-normal solar spectral irradiance according to ASTM G173 (Tables for terrestrial direct normal solar spectral irradiance for air mass 1.5).

Fig. 1. Photographs of galvanised model silos with different outer thermal layers on roof tops of model buildings and a weather station near the model buildings

A Fourier transform infrared (FTIR) spectrometer (Nicolet iS50, Thermo Fisher Scientific, Waltham, MA, USA) equipped with an integrating sphere was employed to characterise the infrared spectra of the coating films in the spectral regions of 2.5–24 μm and 8–14 μm.

An emissometer (AE1, Devices & Services Co., Dallas, TX, USA) was used to measure the overall infrared emissivities of different materials. Another portable emissometer (IR-2, Shanghai Chengbo Optoelectronic Technology Co., Ltd.) was employed to test the emissivity in the atmospheric transparency window (8–14 μm). The accuracy of both emissometers was 0.01.

According to ASTM C-19 (Standard test method for steady-state heat flux measurements and thermal transmission properties by means of the guarded-hot-plate), the thermal conductivity of the coating system was measured using a guarded hot plate (GHP) apparatus (GHP 456 Titan®, Netzsch Analyzing & Testing, Germany). The accuracy was ±2 %.

3.3. Rooftop measurements of the cooling effect

As shown in Fig. 1, four self-developed galvanised steel silos on the rooftops of model buildings located in Longquanyi District, Chengdu, China, were employed to illustrate the cooling effect of the SDRC coating and its faster heat dissipation during the night.

For each silo, the height of the cone part was 0.2 m, and the diameter and height of the cylinder part were 0.8 m and 1.25 m, respectively. One galvanised silo placed on the roof of a concrete model building was painted with the HE coating, and an unpainted silo on the roof of the middle model building was used as the control. Additionally, two galvanised silos on the roof of the third model building were insulated with 10-cm-thick polyurethane (PU), and one silo was also coated with the HE coating. As shown in Figs. 1 and 10-cm-thick polystyrene boards were placed between the rooftops and four silos to minimise thermal conductivity.

3.4. Cooling performance measurements for buildings

As shown in Fig. 2a–d, two single-story brick bungalows, located in the countryside of Dengzhou City, Henan Province, China, were deliberately selected to show the substantial cooling effect of the SSC-HE coating. The dimension of each bungalow was 12 m long × 5.5 m wide × 3.0 m high. Each room contained a glass window (1.4 m wide × 1.5 m high) and a wooden door (0.9 m wide × 2.4 m high). The thickness of the brick walls and prefabricated concrete roofs was 24 and 20 cm, respectively. While the roof and walls of one bungalow were painted with the SSC-HE coating, the walls of the control bungalow were painted with a common white coating and the concrete roof was unpainted. During the testing period, the rooms of two bungalows were closed.

3.5. Cooling performance measurements for chemical pipelines

As can be seen in Fig. 3, two identical carbon steel-based pipelines, installed on the fertilizer production line in Yinchuan, the Ningxia Hui Autonomous Region, were chosen to compare the cooling effect of the SSC-HE coating with other thermal management solutions such as the most commonly used spray water and sunshade. To this end, one pipeline was painted with the SSC-HE coating and exposed to the sky (Fig. 3a), whereas the other unpainted pipeline was positioned under the colour-coated steel sheet roofing and constantly cooled with spray water (Fig. 3b). For the sake of safety, the surfaces temperatures of the pipelines were measured using an infrared thermometer instead of online measurements which generally require electricity and internet.

3.6. Long-term real-world cooling performance measurements

To determine the long-term sub-ambient cooling effect of the HE coating, we purposely selected a distributed TBS (Fig. 4) located in Ziyang, Sichuan Province, China. The HE primer and SSC topcoat were applied to the base station. The photographs of the base station were taken on September 29, 2021 after it was painted with the SSC-HE coating for one month (Fig. 4a and b). After the applications of the coatings for one year, the appearance of the base station was recorded again on August 28, 2022 (Fig. 4c). Concurrently, the temperatures of the ambient air and the top surface of the battery cabinet were constantly monitored and recorded.

Fig. 2. Photographs of (a) the thermometer screen, (b) panorama and front (c) views of a SSC-HE-coated and (d) a white control brick bungalows.

Fig. 3. Photographs of carbon steel-based chemical pipelines with (a) and without (b) the SSC-HE coating.

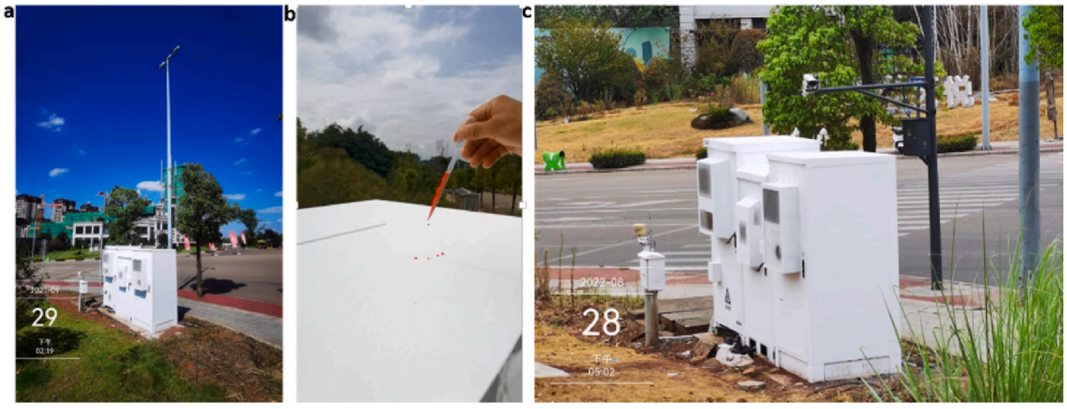

Fig. 4. Photographs of a SSC-HE-coated distributed TBS taken on September 29, 2021 (a and b) and August 28, 2022 (c).

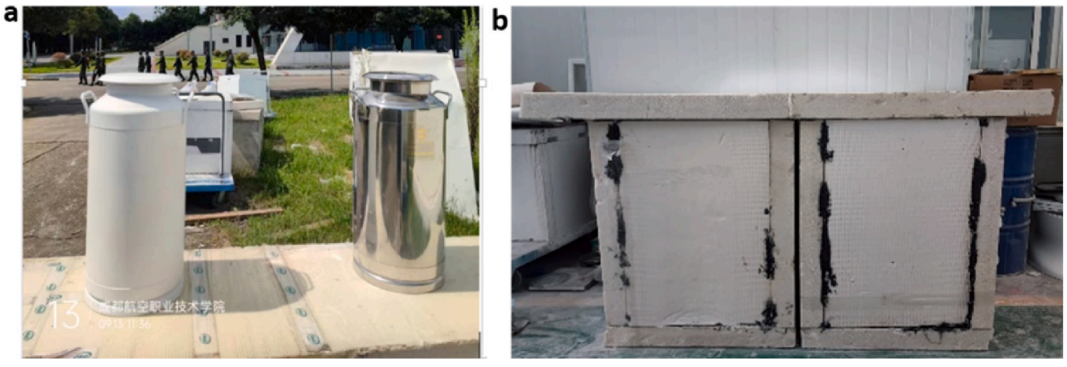

Fig. 5. Photographs of stainless steel milk tanks with and without the HE coating. Heat dissipation measurements were performed in (a) open and (b) adiabatic environments.

3.7. Outdoor and indoor measurements of heat dissipation rates

As shown in Fig. 5, two stainless steel milk-storage tanks placed on top of 10-cm-thick polystyrene boards were applied to demonstrate the SDRC effects of the HE coating and its heat dissipation rate relative to stainless steel in an open environment and the heat dissipation rate inside the building at night (Fig. 5a). Furthermore, the two tanks were individually placed into two insulated boxes composed of 10-cm-thick polystyrene boards (Fig. 5b) to test the heat dissipation rates in adiabatic environments.

3.8. Measurements of heaters

Two concrete-based model single-story buildings with one door were constructed using pre-fabricated concrete structure (Fig. 6a). The dimension of each building was 2.2 m long × 1.6 m wide × 1.6 m high. The thickness of walls and roofs of the buildings was 8 cm. In addition, each model building contained a glass door (1.5 m long × 0.8 m wide).

Three identical electric oil heaters were individually painted with the HE coating and commercially available aluminium and black coatings (Fig. 6b). The maximum output power of the heaters was 2200 W. While the HE-coated heater was consistently placed inside the left model building and used as a reference, the other two were successively placed in the middle of the other model building to compare the heating rates of the model buildings and the heat dissipation rates of the heaters.

3.9. Instrumentation

Sufficient digital temperature–humidity sensors and negative temperature coefficient (NTC) metal-clad thermistors were employed to record the temperatures of the ambient air, silos, milk storage tanks, electric oil heaters, and interior room of the model buildings. The accuracy of temperature sensors was ±0.1 °C.

To test the top and roof surface temperatures of the silos, buildings and the battery cabinet of the distributed TBS, the temperature–humidity sensors were fixed to the tops of the substrates. For the SSC-HE-coated substrates, the upper surfaces of the temperature sensors were covered with the SSC-HE coating. To measure the interior air temperatures of the silos and buildings, sensors were suspended at the centre of the silos and buildings.

To measure the temperatures of the milk storage tanks' top surface, temperature–humidity sensors were fixed on the tops of the tanks, and the sensor on the HE-coated tank was covered with the HE coating. The sensors were immersed in water to measure the temperatures inside the tanks.

To measure room temperatures of the model buildings, NTC thermistors were installed in the centres of the rooms.

In addition, a pyranometer (MS-802, EKO Instruments, Hague, Netherlands) and a temperature sensor fixed in a thermometer screen were used to measure the solar irradiance and temperature of ambient air, respectively. The accuracy was ±10 W/m^2.

Additionally, digital electricity meters were employed to measure the power consumption of the electric oil heaters.

4. Results

4.1. Optical properties of the SSC-HE coating

The thermal properties of a material are mainly determined by its optical features in the solar (0.25–2.5 μm) and infrared (>2.5 μm) regions. Therefore, the spectral reflectance and emissivity in the infrared region between 2.5 and 24 μm for the SSC-HE coating were first characterised, and the results are presented in Fig. 7. The computed solar reflectance and emissivity in the atmospheric transparency window (8–14 μm) of the SSC-HE coating were 0.985 and 0.991, respectively.

Fig. 6. Photographs of concrete model buildings (a) and electric oil heaters (b) pained with the HE, aluminium and black coatings.

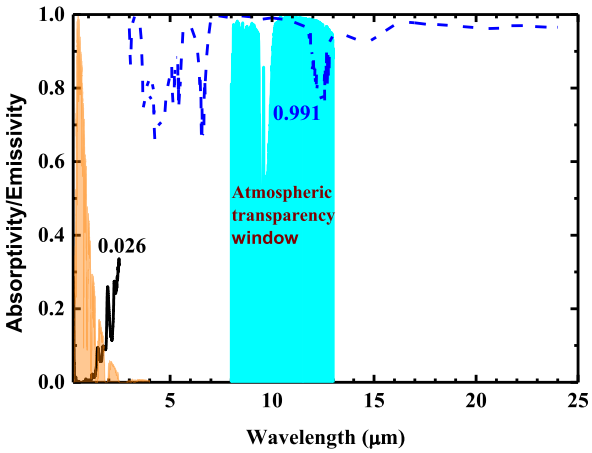

Fig. 7. Absorptivity/Emissivity of the SSC-HE coating measured in the solar and infrared regions.

Table 1
Overall emissivities and those in the atmospheric transparency window for the galvanised steel, stainless steel, and aluminium, black, and HE coatings.

Samples	Emissivity	
	8–14 μm	Overall
Galvanised steel	0.070	0.040
Stainless steel	0.120	0.130
Aluminium paint	0.780	0.650
Black paint	0.860	0.880
SSC-HE coating	0.991	0.920

4.2. Emissivity for different materials

As shown in Eqs. (2) and (3), the emissivity determines the thermal properties of a material. The measured overall emissivity values and those in the atmospheric transparency window for the galvanised steel, stainless steel, and aluminium, black, and SSC-HE coatings are summarised in Table 1. As expected, the emissivities of the metals were low. Additionally, as indicated in Table 1, the emissivities of the different coatings increased in the following sequence: $\varepsilon_{\text{aluminium paint}} < \varepsilon_{\text{black paint}} < \varepsilon_{\text{SSC-HE coating}}$.

4.3. Cooling effect of the SSC-HE coating on well-insulated silos

In addition to the infrared emissivity, another intrinsic metrics determining the thermal properties of a material is its thermal conductivity. The thermal conductivity of the SSC-HE coating was 0.11 $Wm^{-1}K^{-1}$, which was much higher than that of the PU insulation (0.02 $Wm^{-1}K^{-1}$). Moreover, the overall dry coating thickness of the SSC-HE coating system was no thicker than 500 μm.

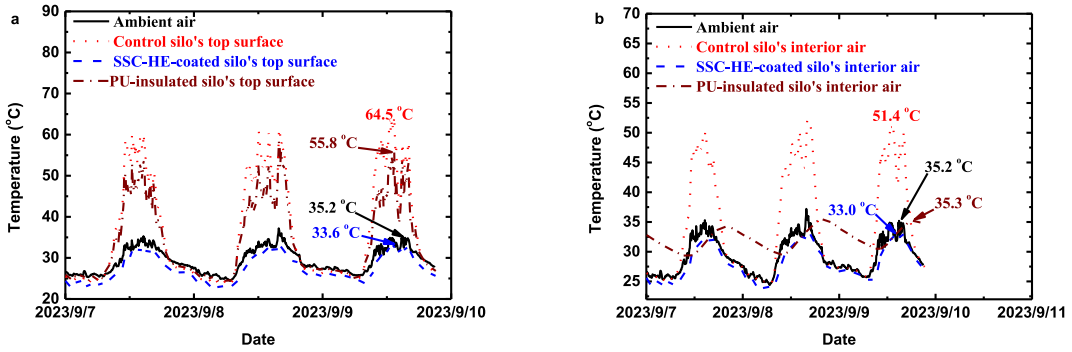

Fig. 8. Temperature data for galvanised model silos with different thermal properties from 7 to September 9, 2023: (a) temperatures of ambient air, top surfaces of the control, SSC-HE-coated and PU-insulated silos; (b) temperatures of ambient air and the interior air of the control, SSC-HE-coated and PU-insulated silos.

Therefore, the cooling effect of a SSC-HE-coated structure exposed to a daylight sky is mainly determined by its solar reflectance and infrared emissivity rather than the thermal conductivity.

Fig. 8 shows the top surface and interior air temperatures of galvanised steel silos with different thermal properties relative to the ambient air temperature from 7 to September 9, 2023. As shown in Fig. 8a, the top surface temperatures of the galvanised-steel-based silo coated with the SSC-HE coating was consistently below the ambient air temperature, indicating prominent SDRC effects. In contrast, the top surface temperatures of the galvanised-steel-based coating was higher than the ambient air temperature during the daytime and below the ambient air temperature at night. At noon on September 9, 2023, when the maximum ambient air temperature was 35.2 °C, the maximum top surface temperature of the SSC-HE-coated silo was 1.6 °C below the ambient air temperature, and it was 30.9 °C lower than that of the control.

During the daytime, the top surface temperatures of the PU-insulated silo was lower compared to that of the control. It is widely accepted that the surface temperature of a material at night is determined by its emissivity. As indicated in Table 1, the overall emissivity and that in the wavelength range of 8–14 μm for the galvanised steel were much lower than those of the HE coating. Therefore, during the night, although the surface temperatures of the galvanised steel and PU-insulated silos were also below the ambient air temperature, they were still higher than that of the HE-coated silo.

As shown in Fig. 8b, in the absence of PU insulation, the HE coating with a consistent sub-ambient surface temperature would subsequently cool the attached galvanised steel structures and interiors through heat transfer to a steady state sub-ambient temperature over time, resulting in the desired system-wide cooling during day and night [2,36,43]. In the presence of 10-cm-thick PU insulation, the SSC-HE coating further reduced the interior air temperature of the silo. However, the interior temperatures of the PU-insulated silo were above the ambient air temperature during the late afternoon and night because of the insulation effect of the PU. Although the interior temperature of the PU-insulated silo was lower than that of the SSC-HE-coated silo at midday, the maximum value of the former in the late afternoon was higher than that of the latter in the early afternoon. On September 9, 2023, when the maximum ambient air temperature was 35.2 °C at midday, the maximum interior temperatures of the HE-coated silo was 2.2 °C lower than the ambient air temperature. In contrast, the maximum interior air temperatures of the control and PU-insulated silo were 0.1 °C and 16.2 °C above the ambient air temperature, respectively. Accordingly, applying the SSC-HE coating reduced the interior air temperature of silo by 18.4 °C.

To study the SDRC effect of the SSC-HE coating on a well-insulated structure, we added a new silo with 10-cm-thick PU insulation interlay and painted it with the SSC-HE coating. Fig. 9 shows the weather, temperatures of the top surface and interior air of galvanised steel silos with different thermal properties against the ambient air temperature from 31 May to June 2, 2024. Under weather conditions indicated in Fig. 9a, the top surface temperatures of both the galvanised-steel-based and PU-insulated silos coated with the SSC-HE paint were consistently lower than the ambient air temperature, with the latter being nearly identical to the former, indicating

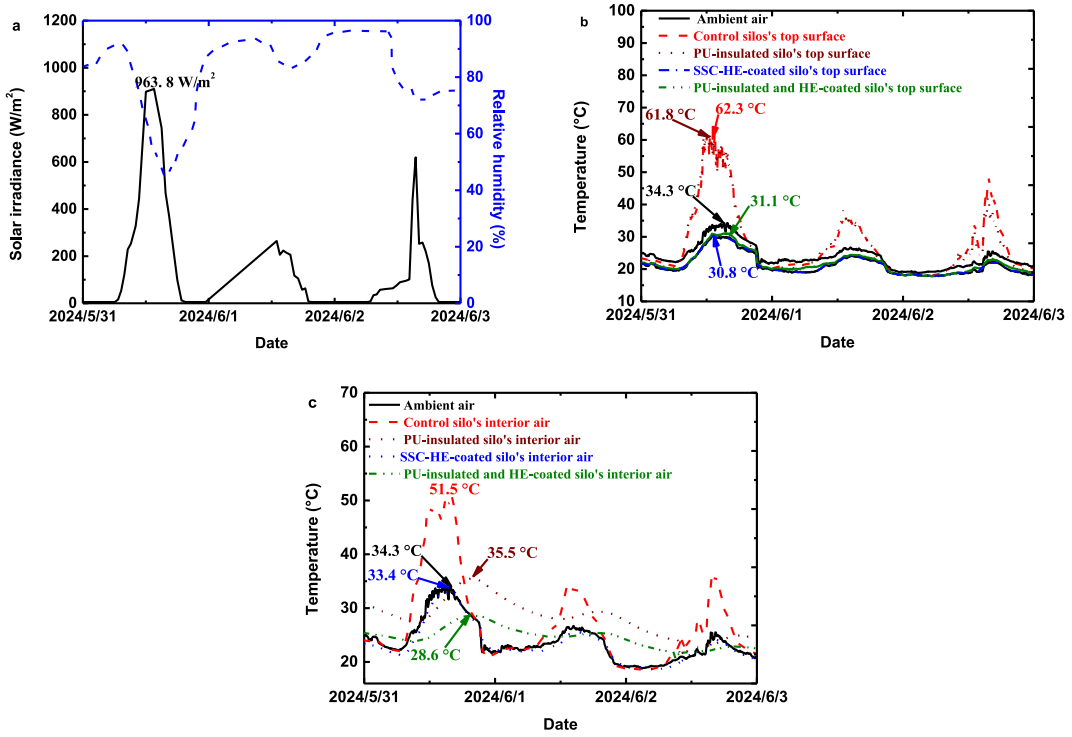

Fig. 9. (a) Solar irradiation and relative humidity from 31 May to June 3, 2024. (b)Temperatures of ambient air and top surface of the galvannized steel-based, PU-insulated, SSC-HE-coated and both PU-insulated and SSC-HE-coated model silos. (c) Temperautes of ambient air and interior air of galvanised steel-based, SSC-HE-coated and both PU-insulated and SSC-HE-coated model silos.

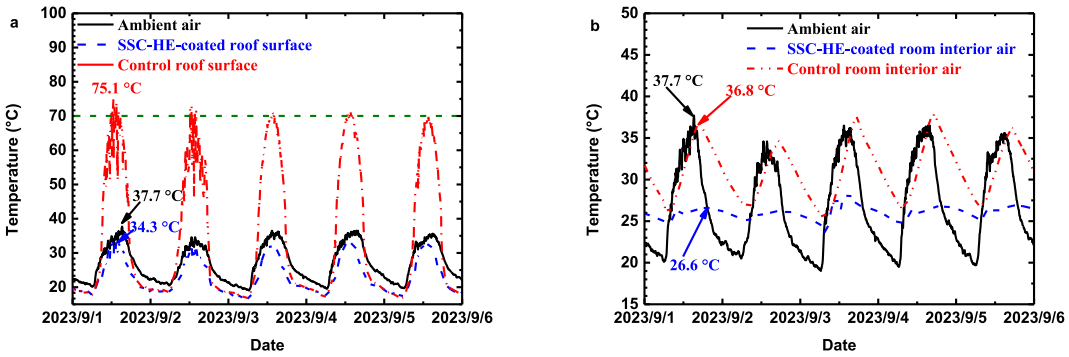

Fig. 10. Temperature data for brick bungalows from 1 to September 5, 2023: (a) temperatures of ambient air, roof surfaces of the control and SSC-HE-coated brick bungalows; (b) temperatures of ambient air and the room interior air of the control and SSC-HE-coated bungalows.

prominent SDRC effects. In contrast, the surface temperatures of the galvanised-steel-based and PU-insulated silos without the SSC-HE coating were substantially higher than the ambient air temperature under direct sunlight and below the ambient air temperature during the night. At noon on May 31, 2024, when the maximum temperature of ambient air was 34.3 °C, the maximum cooling effect of the SSC-HE coating on the galvanised silo was 3.5 °C below the temperature of ambient air, and the top surface temperature of the SSC-HE-coated silo was 31.5 °C lower than that of the counterpart. Concurrently, the maximum temperature reduction of the silo that was painted with the SSC-HE coating and insulated with PU was 3.2 °C below the ambient air temperature, and its top surface temperature was reduced by 30.7 °C as compared to the PU-insulated silo (Fig. 9b).

As shown in Fig. 9c, in the absence of PU insulation, the interior air temperature of the SSC-HE-coated silo was consistently below that of the ambient air. In the presence of 10-cm-thick PU insulation, the SSC-HE coating further decreased the interior air temperature of the silo. However, the interior air temperatures of the PU-insulated silo and the silo with SSC-HE coating and PU insulation were above that of the ambient air during the late afternoon and night because of the insulation effect of the PU. On May 31, 2024, when the maximum ambient air temperature and solar irradiation were 34.3 °C and 963.8 W/m^2 (Fig. 9a) at midday, respectively, the maximum interior air temperatures of the SSC-HE-coated silo with and without PU insulation were 5.7 °C and 0.9 °C lower than the ambient air temperature, respectively. In contrast, the maximum interior air temperatures of the control and PU-insulated silo without the SSC-HE coating were 17.2 °C and 1.2 °C above the ambient air temperature, respectively. Accordingly, applying the SSC-HE coating reduced the interior air temperature of silos with and without PU insulation by 6.9 °C and 22.9 °C, respectively. In terms of cooling, the SSC-HE coating was more effective than the 10-cm-thick PU, except at midday. Additionally, even in the presence of 10-cm-thick PU insulation, the HE coating still exhibited a pronounced cooling effect.

4.4. Sub-ambient coolindg effect for brick bungalows

As mentioned above, both the roof surface and room temperatures of SSC-HE-coated concrete and carbon steel-based prefabricated houses showed remarkable sub-ambient cooling effect [34,35]. In addition to these two types of buildings, brick bungalows are probably the most common civilian houses in the countryside in the north of China. Therefore, the SSC-HE coating was applied to a brick bungalow and the cooling effect was investigated.

Fig. 10 shows the temperatures of the ambient air, roof surface and room interior air of the SSC-HE-coated and control brick bungalows. As shown in Fig. 10a, during five consecutive sunny days in the early autumn 2023, while the concrete roof surface temperature of the control bungalow was much higher than the ambient air temperature, the SSC-HC-coated roof surface temperature was constantly below the ambient air temperature, showing distinguished sub-ambient cooling effect day and night. On September 1, 2021 when the naximum ambient air temperature was 37.7 °C,the SSC-HE-coated roof surface temperature was 34.3 °C, which was 3.4 and 40.8 °C lower than the ambient air and the control concrete roof surface temperatures, respectively.

As a consequence of the thermal conduction and convection, the room interior air temperature of the SSC-HE coated bungalow showed sub-ambient cooling effect during the daytime. Because of the heat preservation effect of the building envelope, the roon temperatures of both the SSC-HE coated and control bangalow were above the ambient air temperature (Fig. 10b). On September 1, 2023, the maximum room interior air temperature of the SSC-HE-coated bungalow was 26.6 °C, which was 11.1 and 10.2 °C lower than the maximum ambient air (37.7 °C) and control (36.8 °C)temperatures, respectively. During the remaining four days, the maximum room interior air temperature of the SSC-HE-coated bungalow was lower than 28.0 °C. Obviously, the cooling performance of the SSC-HE coating could nearly meet the higher requirements of the thermal managements of buildings in summer.

4.5. Comparison of cooling effects with sunshade and spray water

Currently, sunshade and spray water are commonly employed to protect chemical pipelines and oil storage tanks from overheat resulted from the solar irradiation in summer. As shown in Video S1, the measured surface temperature of the SSC-HE-coated pipeline was 34 °C, which was 7 °C lower than that of the unpainted pipeline (41 °C). Note that the unpainted pipeline was not only under the

sunshade but also constantly sprayed water. Apparently, the cooling effect of the SSC-HE coating was better than the combination of the sunshade and spray water. After all, the extremely high solar reflectance of 0.985 and overall infrared emissivity of 0.92 of the SSC-HE coating enabled the surface temperature of the coated pipeline to be constantly lower than the ambient air temperature, whereas the sunshade and spray water could only allow the surface temperature of the pipeline to be at most identical with the ambient air temperature.

4.6. Long-term sub-ambient cooling effect under real working conditions

For a super-cool surface with sub-ambient temperature, extensive dew formation is unavoidable and dewdrops precipitate dirt [7], resulting in the attenuation of the solar reflectance and thus the loss of the sub-ambient cooling. To protect the HE-coated surface from contamination, the SSC coating was introduced as the topcoat. Fig. 11 shows the solar irradiance and temperatures of the ambient air and top surface for a SSC-HE-coated distributed TBS after it was painted for one and twelve months.

On clear sunny days in September 2021 and August 2022, the top surface temperatures of the battery cabinet were consistently lower than the ambient air temperature, showing typical sub-ambient cooling effect. On September 19, 2021 when the maximum solar irradiance was 770 W/m^2, the sub-ambient cooling effect of the coating was 5.3 °C (Fig. 11a). On August 22, 2022 when the maximum solar irradiance was 766 W/m^2, the sub-ambient temperature reduction of the coating was 5.1 °C. Apparently, the attenuation of the sub-ambient cooling effect is negligible. Additionally, as shown in Fig. 4, the distributed TBS was still spotless even after one year because of the presence of the SSC topcoat.

4.7. Heat dissipation rate of the HE coating

Freshly squeezed milk has a temperature of approximately 38 °C, which is the most appropriate temperature for microbial growth. However, in grasslands, milking generally starts at 8 a.m. and is sustained for a period of time, during which the ambient temperature rapidly rises, resulting in a continuous temperature increase of the milk.

Fig. 12a shows the temperatures of ambient air and top surfaces of the unpainted milk storage tank and that pained with the SSC-HE coating. While the moderate solar reflectance and ultralow emissivity of the stainless steel ensured the top surface temperature of the unpainted milk storage tank was always above the ambient air temperature throughout the day, the extremely high solar reflectance and emissivity of the SSC-HE coating enabled the coated tank to show prominent sub-ambient cooling effects during the day and night.

Fig. 12b presents the time dependence of the temperatures of the ambient air and top surfaces of the two milk storage tanks filled with water at 40 °C. As indicated in Fig. 12b, the top surface temperature of the SSC-HE-coated tank was initially above the ambient temperature because of the addition of the hot water, and it subsequently dropped below the ambient air temperature. In contrast, the top surface temperature of the control tank continuously increased to the maximum value of 53.9 °C, which was substantially higher than the maximum ambient air temperature of 33.8 °C and was 21.6 °C higher than the maximum top surface temperature of the SSC-HE-coated tank (32.3 °C).

Consequently, while the temperature of the water inside the control tank primarily decreased and eventually increased to 40.6 °C at noon, the temperature of water in the SSC-HE-coated tank continually decreased to 31.9 °C, yielding a temperature decrease of 8.7 °C (Fig. 12c). The heat dissipation effect of the SSC-HE coating during the daytime is thus immediately obvious. The excellent daytime heat dissipation capacity of the SSC-HE coating can be attributed to both its high solar reflectance and high emissivity.

The concept of emissivity in the atmospheric transparency window generally misleads one into the belief that surface materials can maximally dissipate heat only when placed outdoors. To demonstrate the contribution of emissivity to heat dissipation and radiative cooling, we placed the two milk storage tanks mentioned above in a building and tested the heat dissipation rate in the evening. The results are presented in Fig. 13. Unexpectedly, while the temperature of the hot water inside the SSC-HE-coated tank deceased from 58.7 °C to 20.7 °C, that inside the control tank decreased more slowly from 58.9 °C to 27.7 °C in the same time, resulting in a final temperature difference of 7 °C. This new result indicates that facing the sky may not necessarily be a prerequisite for a surface material to maximally dissipate heat.

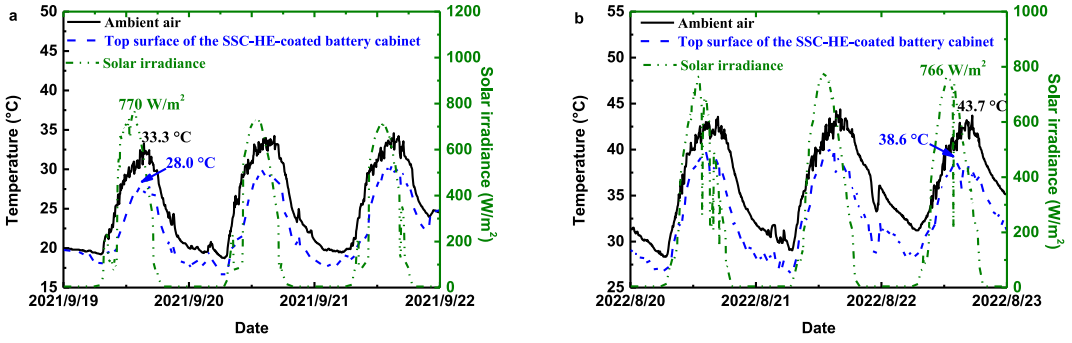

Fig. 11. (a) Solar irradiation, ambient air and top surface temperatures for the battery cabinet of a SSC-HE-coated distributed TBS during the testing period from (a) 19 to September 21, 2021 and (b) 20 to August 22, 2022.

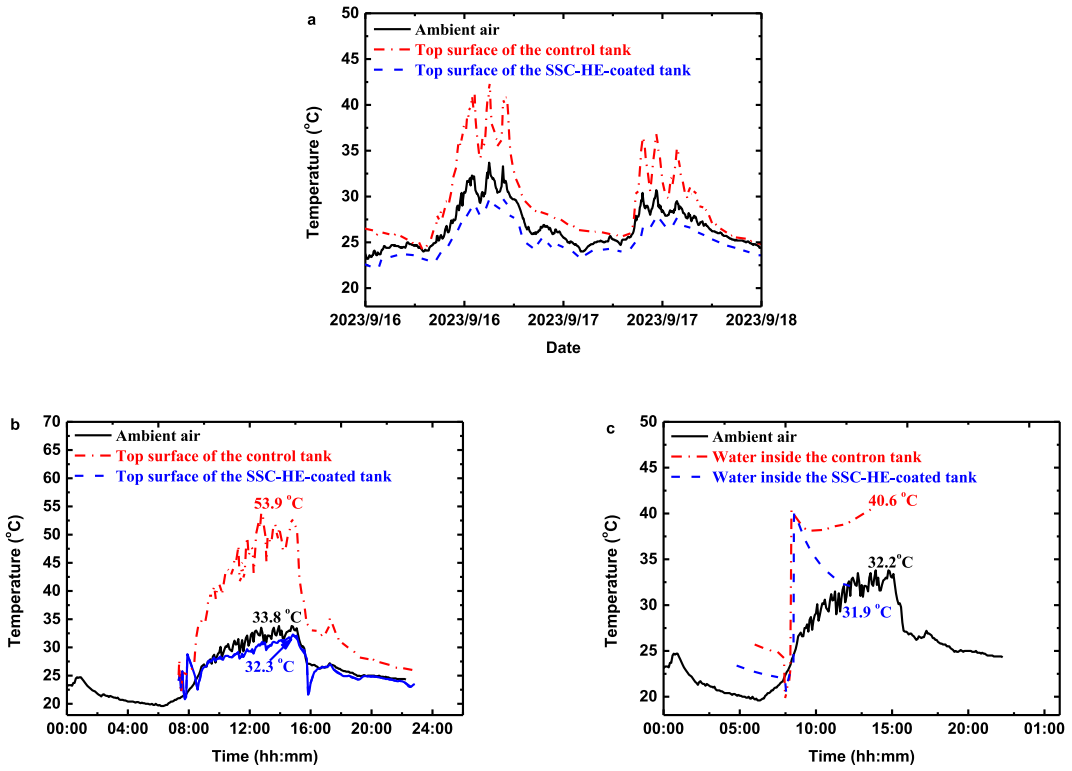

Fig. 12. Temperature data for stainless steel milk storage tanks: (a) temperatures of ambient air and top surface s of the control and SSC-HE-coated tanks from 16 to September 17, 2023; (b) temperatures of ambient air and top surface of the control and SSC-HE-coated tanks measured on September 14, 2023; (c) temperatures of ambient air and water inside the control and HE-coated tanks measured on September 14, 2023.

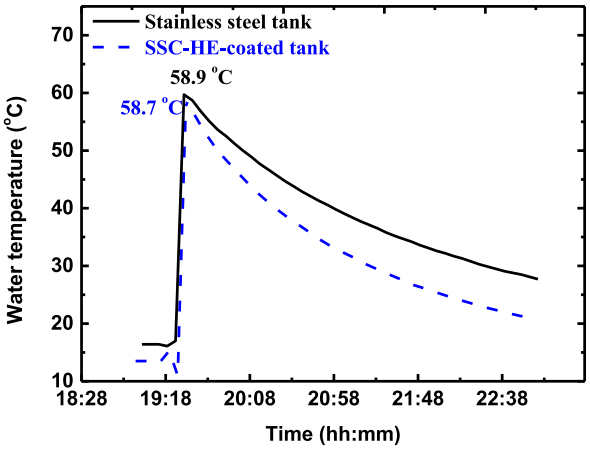

Fig. 13. Comparison of the heat dissipation rates of the stainless steel milk storage tanks in the indoor environment, showing the time dependence of the water temperatures inside the control and SSC-HE-coated stainless steel milk tanks.

To validate the above theory, we placed the two milk-storage tanks in two insulated boxes to test the heat dissipation rates, and the results are shown in Fig. 14. Under adiabatic conditions, compared with the control tank, the temperature of water in the SSC-HE-coated tank decreased more rapidly from the same initial temperature of 88.8 °C to a final temperature of 34.8 °C, which was 12.4 °C lower than that of the water in the control tank.

These observations demonstrate that a surface material with higher emissivity must necessarily show a better heat dissipation effect, which is not only independent of the environment in which the material is located, but also independent of the solar reflectivity of the material. SSC-HE coatings can be applied to many objects and locations to meet the cooling and heat dissipation requirements of users.

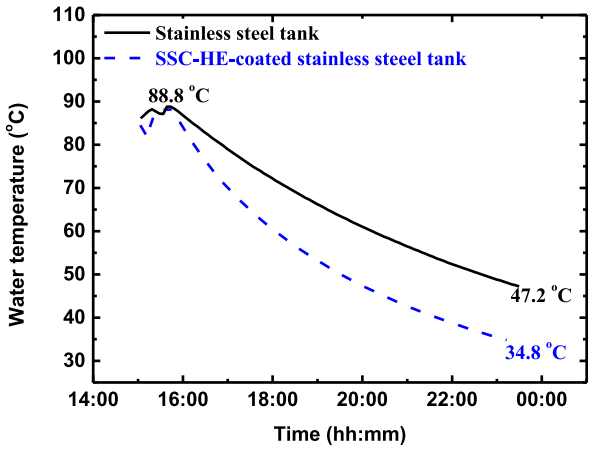

Fig. 14. Comparison of the heat dissipation rates of stainless steel milk storage tanks under adiabatic conditions, showing the time dependence of the water temperature in the control and SSC-HE-coated stainless steel milk tanks.

4.8. Applications to heating radiators

Inspired by the above experimental results, we applied the HE coating to an electric oil heater and investigated its potential to improve the thermal comfort and conserve the heating energy consumption of a building. To this end, we first calibrated the room temperatures of two identical model buildings; the results are presented in Fig. 15a. As can be seen in Fig. 15a, the two curves nearly overlap. Within experimental error, the room temperatures of the two model buildings were identical.

First, we investigated the heating effects of the HE- and aluminium-coated electric oil heaters. Maintaining identical room temperatures of the two model buildings (Fig. 15b), we measured the accumulated electricity consumption of the HE- and aluminium-coated heaters installed in the two model buildings; the results are presented in Fig. 15c. Here, we define the heating energy efficiency (*HEE*) as the percentage ratio of the heating energy consumption (*HEC*) difference between the heater with lower emissivity (HEC_1) and the HE-coated heater (HEC_2) to HEC_1, as follows:

$$HEE = \frac{HEC_1 - HEC_2}{HEC_1} \times 100\% \tag{1a}$$

As shown in Fig. 15c, the HE-coated heater consumed 0.4 kW h less heating power, yielding an *HEE* of 5.9 %.

Subsequently, two electric oil heaters were operated for a period of time at an identical maximum output power of 2200 W, and the power consumption of the heaters and the room temperature were measured; the results are shown in Fig. 15d and e, respectively. Under nearly identical power consumptions (Fig. 15d), the room temperature of the model building with the HE-coated electric oil heater increased faster, and the equilibrium temperature was higher than that of the model building with the aluminium-coated heater (Fig. 15e). The average equilibrium temperature of the model building with the HE-coated heater was 2.1 °C higher than that of the counterpart building.

Subsequently, we determined and compared the heating effects of the heaters painted with HE and black coatings. The results are presented in Fig. 16. As shown in Fig. 16a, under an identical room temperature setting, the model building with the HE-coated heater reached the equilibrium room temperature earlier (by 111 min) than the model building with the black heater. The HE-coated heater consumed 0.4 kW h less heating power than the black heater under identical room temperature settings, generating an *HEE* of 4.4 % (Fig. 16b).

While employing two electric oil heaters to heat the model buildings at maximum output power for several hours, we measured the heating power consumption of the two heaters and the room temperatures of the model buildings. The results are presented in Fig. 16c and d. Under identical heating power consumption levels (Fig. 16c), the model building with the HE-coated heater reached an average equilibrium temperature that was 1.9 °C higher than that of the model building with the black heater (Fig. 16d). Because the difference in emissivity between the HE and the black coating (0.04) was smaller than that between the HE and the aluminium coating (0.27), the heating energy efficiency of the HE-coated heater relative to the black heater (4.4 %) was smaller than that of the HE-coated heater relative to the aluminium-coated heater (5.9 %). Thus, the average equilibrium temperature difference of the model buildings in the former case (1.9 °C) was lower than that in the latter case (2.1 °C).

5. Discussion

As indicated in Table 1, the infrared emissivity and the emissivity in the atmospheric transparency window of the SSC-HE coating were 0.92 and 0.991, respectively, which were much higher than those of galvanised steel (0.04 and 0.07) and stainless steel (0.13 and 0.12). Therefore, at night, the surface and interior air temperatures of the SSC-HE-coated galvanised steel silo and SSC-HE-coated PU-insulated galvanised steel silo were lower than those of their corresponding counterparts. Moreover, compared with the stainless steel

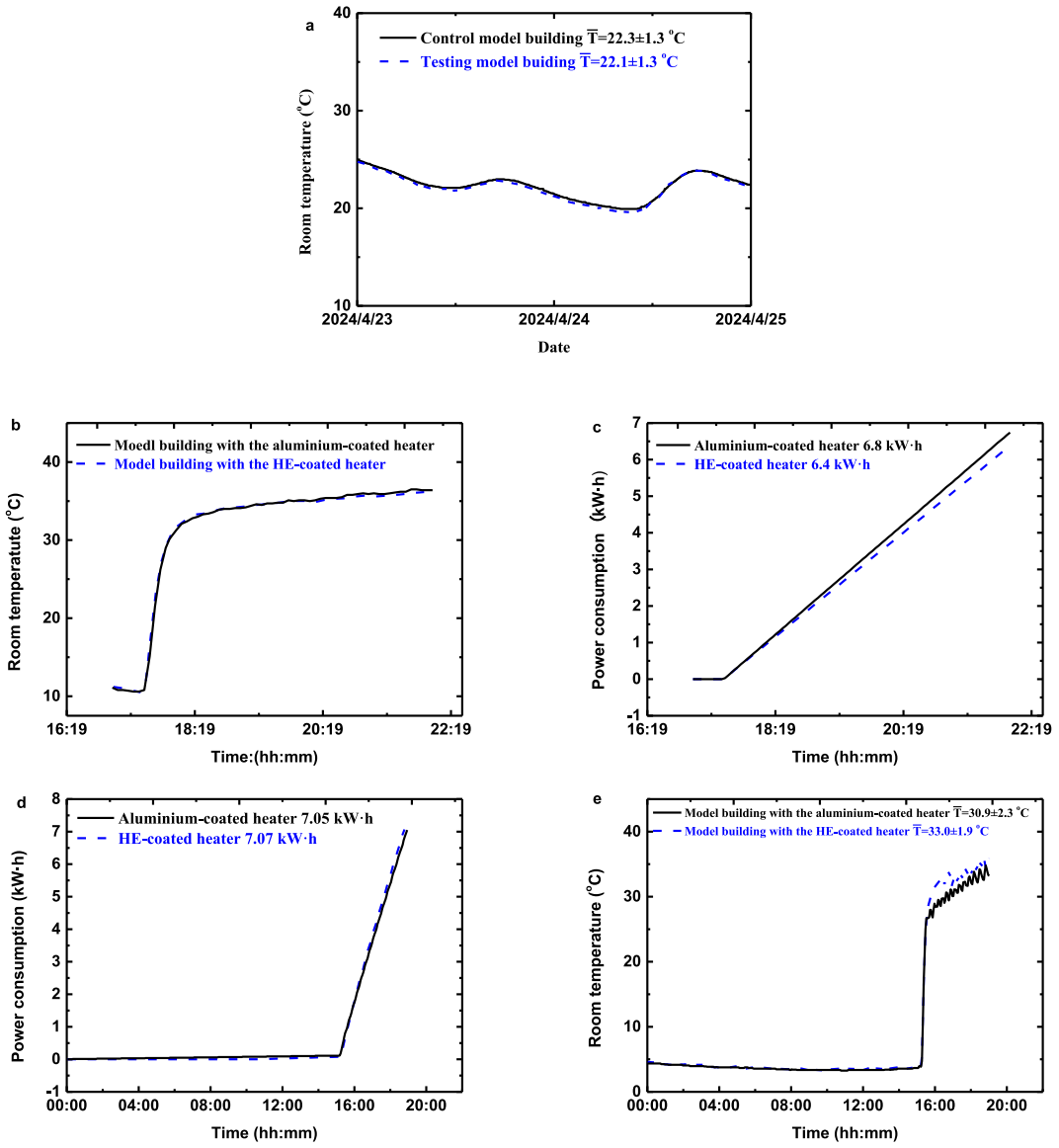

Fig. 15. (a) Comparison of the room temperatures of the control and testing model buildings from 23 to April 24, 2024. (b) Room temperatures of concrete model buildings with aluminium- and HE-coated electric oil heaters on January 25, 2024. (c) Accumulated power consumptions of aluminium- and HE-coated electric oil heaters on January 25, 2024. (d) Accumulated power consumptions of aluminium- and HE-coated electric oil heaters on January 24, 2024. (e) Room temperatures of concrete model buildings with aluminium- and HE-coated electric oil heaters on January 24, 2024.

milk storage tank, the HE-coated milk storage tank showed better heat dissipation performance owing to the much higher infrared emissivity of the SSC-HE coating.

To explain the better heating effect of the HE-coated electric oil heater relative to the black heater, we measured the surface temperatures of these two heaters under identical room temperature settings on February 1, 2024 and identical maximum output power consumptions on February 4, 2024, and the results are shown in Fig. 17. As can be seen in Fig. 17a, the average equilibrium surface temperature of the HE-coated and black heaters were nearly identical on February 1, 2024 when the room temperatures of two model buildings were identical. As can be seen from Fig. 17b, the average equilibrium surface temperature of the HE-coated heat was 9.0 °C higher than that of the black heater on February 4, 2024 when the two heater worked at the identical maximum output power. According to Eq. (3), as compared to the black heater, at the same surface temperature of the heaters, the HE-coated heater released heat faster than the black one did; at the same maximum output power, more heat from the HE-coated heater was lost and transferred to the surrounding environment, which resulted in a higher equilibrium temperature of the model building.

As shown above, the SSC-HE coating can effectively decrease the surface and interior air temperatures of the system during day and night. Therefore, it has been widely applied to buildings for thermal comfort or cooling energy efficiency in summer, grain warehouses

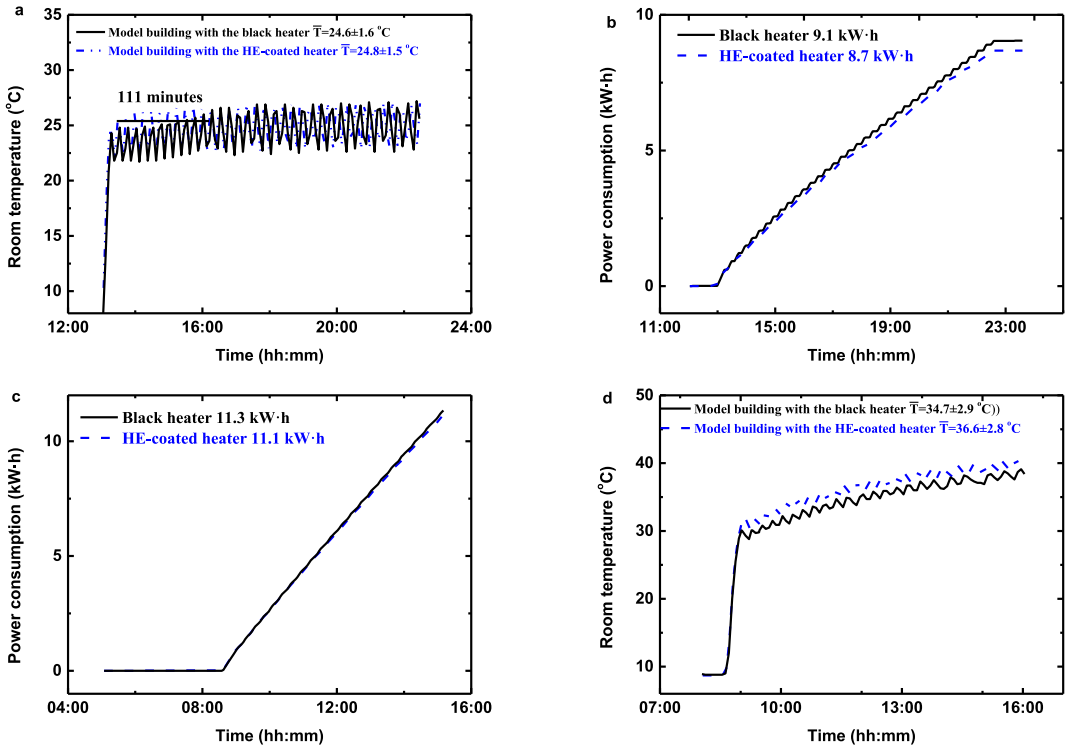

Fig. 16. Power consumption and temperature data: (a) room temperatures of concrete model buildings with black and HE-coated electric oil heaters on January 30, 2024; (b) accumulative power consumptions of the black and HE-coated electric oil heaters on January 30, 2024; (c) accumulative power consumptions of the black and HE-coated electric oil heaters on February 2, 2024; (d) room temperatures of concrete model buildings with black and HE-coated electric oil heaters on February 2, 2024.

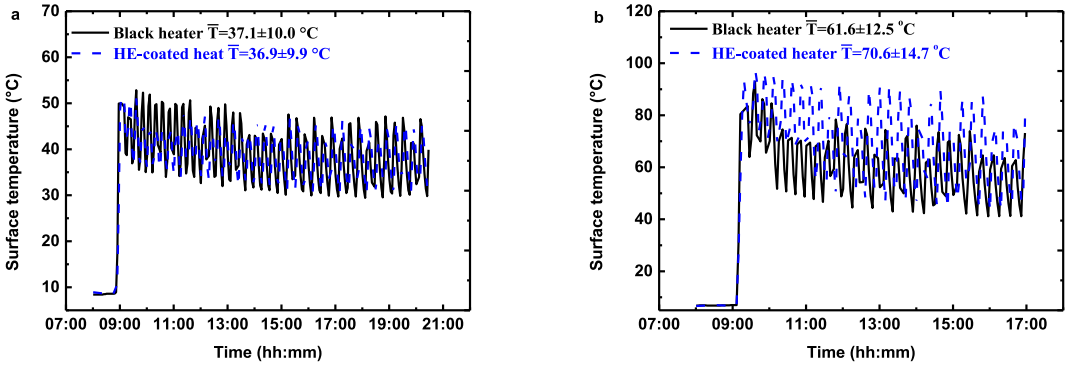

Fig. 17. Temperature data on 1 (a) and 4 (b) February 2024: surface temperatures of the black and HE-coated electric oil heaters.

for low-temperature storage of grains, oil and gas storage tanks for storage safety and energy savings, and telecommunications and power facilities for operation safety and cooling energy conservation.

Because the HE coating can also reduce the temperature of the attached structure at night regardless of its location, it has great potential for use in mechanical and electronic equipment, heat sinks, and condensers for heat dissipation. Additionally, the HE coating can be utilised in different types of heaters to improve thermal comfort and reduce heating energy consumption in winter. In other words, without any external energy input, the HE coating can be employed to reduce both cooling and heating energy consumption.

6. Conclusions

The experimental results presented above allowed us to draw the following conclusions can be summarised.

In terms of cooling, the SSC-HE coating was more effective than 10-cm-thick polyurethane except at midday. The maximum interior air temperature of the SSC-HE-coated silo could be 2.3 °C lower than that of the PU-insulated silo.

When applied to a well-insulated system such as a metal silo with 10-cm-thick PU insulation, the SSC-HE coating still exhibited remarkable daytime radiative cooling effect of 3.2 °C below the ambient air temperature. On a clear summer sunny day with the maximum ambient air temperature of 34.3 °C, the SSC-HE coating decreased the interior air temperature of the PU-insulated silo by as much as 6.9 °C; and the interior air temperature of the SSC-HE-coated and PU-insulated silo was 22.9 °C lower than that of the counterpart.

For brick bungalows, the SSC-HE coating significantly reduced the roof surface and room interior air temperatures and enabled them to be below the ambient air temperature, showing remarkable sub-ambient cooling effects. The room interior air temperature could be reduced by 11.1 °C. Moreover, compared with the sunshade and spray water, the SSC-HE coating showed better cooling effect. In addition, the introduction of SSC topcoat endowed the HE coating with superomniphobic self-cleaning property. After the outdoor exposure for one year, the battery cabinet of the SSC-HE-coated TBS was still stainless and the sub-ambient cooling effects did not attenuate.

When applied to metal containers and equipment, the SSC-HE coating exhibited excellent heat dissipation effects during the day and night, regardless of the facility location. Under adiabatic conditions, relative to an open environment, the SSC-HE-coated metal facilities dissipated heat more efficiently.

When utilised in heaters, HE coating could facilitate heat transfer, increase the equilibrium room temperature, improve the thermal comfort of buildings, and reduce the heating energy consumption. Relative to the aluminium- and black paint-coated electric oil heaters, the HEE of the HE-coated heater was 5.9 % and 4.4 %, respectively.

In a word, the HE coating can be employed to reduce both the cooling and heating energy consumption of buildings.

Data availability

Data will be made available on request.

CRediT authorship contribution statement

Zhuo Yang: Methodology, Investigation, Data curation. **Zhangran Yang:** Methodology, Investigation. **Zihan Zhang:** Software, Investigation. **Yuanzhu Cai:** Investigation. **Xingjian Wang:** Investigation. **Yanwen Li:** Investigation. **Ruohan Zhang:** Methodology. **Yangang Zhang:** Methodology. **Lianhua Liu:** Project administration. **Weidong Zhang:** Writing – review & editing, Writing – original draft, Methodology, Funding acquisition, Formal analysis, Data curation, Conceptualization. **Lijin Xu:** Supervision. **Peng Wang:** Supervision.

Declaration of competing interest

The authors declare the following financial interests/personal relationships which may be considered as potential competing interests:

No, we do not have. If there are other authors, they declare that they have no known competing financial interests or personal relationships that could have appeared to influence the work reported in this paper.

Acknowledgements

This work was supported by the financial support provided by Key R&D Program of China Southwest Architectural Design and Research Institute Co., Ltd. (R-2021-01-MS-A-2023) and the financial support provided by China Green Building Engineering Research Centre (Green Building Envelop Technology) (CSCEC-PT-006)

Appendix A. Supplementary data

Supplementary data to this article can be found online at https://doi.org/10.1016/j.heliyon.2024.e38233.

References

[1] C. Wang, K. Pattawi, H. Lee, Energy Saving Impact of Occupancy-Driven Thermostat for Residential Buildings, vol. 211, 2020 109791.
[2] A.P. Raman, M.A. Anoma, L. Zhu, E. Rephaeli, S. Fan, Passive radiative cooling below ambient air temperature under direct sunlight, Nature 515 (2014) 540–544.
[3] A.W. Harrison, M.R. Walton, Radiative cooling of TiO_2 white paint, Sol. Energy 20 (1978) 185–188.
[4] X.Y. Li, J. Peoples, Z.F. Huang, et al., Full daytime sub-ambient radiative cooling in commercial-like paints with high figure of merit, Cell Reports Physical Science 1 (2020) 100221.
[5] J. Mandal, Y. Yang, N. Yu, et al., Paints as a scalable and effective radiative cooling technology for buildings, Joule 4 (2020) 1350–1356.
[6] H. Zhang, Y. Cai, L. Liu, J. Qin, Y. Li, Z. Yang, Z. Sun, R. Wang, Y. Zhang, Y. Feng, Z. He, W. Zhang, C. Feng, X. Xu, Superamphiphobic coatings with subambient daytime radiative cooling—part 1: optical and self-cleaning features, Sol. Energy Mater. Sol. Cells 245 (2022) 111859.
[7] A.R. Gentle, G.B. Smith, A subambient open roof surface under the mid-summer sun, Adv. Sci. 2 (2015) 1500119.

[8] P.C. Hsu, A.Y. Song, P.B. Catrysse, C. Liu, Y. Peng, J. Xie, S. Fan, Y. Cui, Radiative human body cooling by nanoporous polyethylene textile, Science 353 (2016) 1019–1023.
[9] Z. Jurado Kou, Z. Chen, et al., Daytime radiative cooling using near-black infrared emitters, ACS Photonics 4 (2017) 626–630.
[10] Y. Zhai, Y. Ma, S.N. David, D. Zhao, R. Lou, G. Tan, R. Yang, X. Yin, Scalable-manufactured randomized glass-polymer hybrid metamaterial for daytime radiative cooling, Science 355 (2017) 1062–1066.
[11] J. Mandal, Y. Fu, A. Overvit, M. Jia, K. Sun, N. Shi, H. Zhou, X. Xiao, N. Yu, Y. Yang, Hierarchically. Hierarchically porous polymer coatings for highly efficient passive daytime radiative cooling, Science 362 (2018) 315–319.
[12] T. Li, Y. Zhai, S. He, W. Gan, L. Hu, A radiative cooling structural material, Science 364 (2019) 760–763.
[13] X. Xue, M. Qiu, Y. Li, Q.M. Zhang, S. Li, Z. Yang, C. Feng, W. Zhang, J.G. Dai, D. Lei, W. Jin, L. Xu, T. Zhang, J. Qin, H. Wang, S. Fan, Creating an eco-friendly building coating with smart sub-ambient radiative cooling, Adv. Mater. 32 (2020) 1906751.
[14] Y. Yang, L. Long, S. Meng, N. Denisuk, L. Wang, Y. Zhu, Bulk material based selective infrared emitter for sub-ambient daytime radiative cooling, Sol. Energy Mater. Sol. Cells 211 (2020) 110548.
[15] X. Wang, X. Liu, Z. Li, H. Zhang, Z. Yang, H. Zhou, T. Fan, Scalable flexible hybrid membranes with photonic structures for daytime radiative cooling, Adv. Funct. Mater. 30 (2020) 1907562.
[16] Y. Chen, B. Dang, J. Fu, C. Wang, H. Li, Cellulose-based hybrid structural material for radiative cooling, Nano Lett. 21 (2021) 397–404.
[17] T. Wang, Y. Wu, L. Shi, X. Hu, M. Chen, L. Wu, A structural polymer for highly efficient all-day passive radiative cooling, Nat. Commun. 12 (2021) 365.
[18] X.Y. Li, J. Peoples, P. Yao, X. Ruan, Ultrawhite $BaSO_4$ paints and films for remarkable daytime subambient radiative cooling, ACS Appl. Mater. Interfaces 13 (2021) 21733–21739.
[19] S. Zeng, S. Pian, M. Su, Z. Wang, G. Tao, Hierarchical-morphology metafabric for scalable passive daytime radiative cooling, Science 373 (2021) 692–696.
[20] Z. Cheng, H. Han, F. Wang, Y. Yan, X. Shi, H. Liang, X. Zhang, Y. Shuai, Efficient radiative cooling coating with biomimetic human skin wrinkle structure, Nano Energy 89 (2021) 106377.
[21] D. Chae, S. Son, H. Lim, P.-H. Jung, J. Ha, H. Lee, Scalable and paint-format microparticle-polymer composite enabling high-performance daytime radiative cooling, Matter, Today Phys. 18 (2021) 100389.
[22] H. Lim, D. Chae, S. Son, J. Ha, H. Lee, $CaCO_3$ micro particle-based radiative cooling device without metal reflector for entire day, Mater. Today Commun. 32 (2022) 103990.
[23] C. Lin, Y. Li, C. Chi, Y.S. Kwon, J. Huang, Z. Wu, J. Zheng, G. Liu, C. Tso, C.Y.H. Chao, B. Huang, A Solution-processed inorganic emitter with high spectral selectivity for efficient subambient radiative cooling in hot humid climates, Adv. Mater. 34 (2022) 2109350.
[24] M. Chen, D. Pang, H. Yan, Highly solar reflectance and infrared transparent porous coating for non-contact heat dissipations, iScience 25 (2022) 104726.
[25] J. Huang, D. Fan, Core-shell microspheres hybridized membrane for light emitting and radiative cooling, J. Alloys Compd. 924 (2022) 166480.
[26] S. Dong, Q. Wu, W. Zhang, G. Xia, L. Yang, J. Cui, Slippery passive radiative cooling supramolecular siloxane coatings, ACS Appl. Mater. Interfaces 14 (2022) 4571–4578.
[27] J. Song, W. Zhang, Z. Sun, M. Pan, F. Tian, X. Li, M. Ye, X. Deng, Durable radiative cooling against environmental aging, Nat. Commun. 13 (2022) 4805.
[28] X. Zhao, T. Li, H. Xie, H. Liu, L. Wang, Y. Qu, S. Li, S. Liu, A. Brozena, Z. Yu, J. Srebric, L. Hu, A solution-processed radiative cooling glass, Science 382 (2023) 684–691.
[29] K. Lin, S. Chen, Y. Zeng, T. Ho, Y. Zhu, X. Wang, F. Liu, B. Huang, C. Chao, Z. Wang, C. Tso, Hierarchically structured passive radiative cooling ceramic with high solar reflectivity, Science 382 (2023) 691–697.
[30] J. Huang, M. Li, D. Fan, Core-shell particles for devising high-performance full-day radiative cooling paint, Appl. Mater. Today 25 (2021) 101209.
[31] J. Huang, D. Fan, Q. Li, Structural rod-like particles for highly efficient radiative cooling, Matter, Today Energy 25 (2022) 100955.
[32] Z. He, Y. Li, Y. Zhang, X. Xue, Z. Yang, H. Wang, C. Wang, J. Qin, Y. Feng, W. Zhang, L. Xu, Waterborne coatings with sub-ambient cooling under direct sunlight–Part II: cooling effect under real working conditions and key physical properties, Sol. Energy Mater. Sol. Cells 215 (2020) 110665.
[33] L. Liu, H. Zhang, Y. Cai, Y. Li, J. Qin, Z. Yang, R. Wang, Y. Zhang, Z. Sun, X. Xue, Y. Feng, Z. He, W. Zhang, C. Feng, Q. Gao, Superamphiphobic coatings with subambient daytime radiative cooling—part 2: cooling effect under real conditions, Sol. Energy Mater. Sol. Cells 241 (2022) 111736.
[34] Y. Zhang, Z. Yang, Z. Zhang, Y. Cai, Z. Sun, H. Zhang, Y. Li, L. Liu, W. Zhang, X. Xue, L. Xu, Sub-ambient cooling effect and net energy efficiency of a super-amphiphobic self-cleaning passive sub-ambient daytime radiative cooling coating applied to various buildings, Energy Build. 284 (2023) 112702.
[35] Y. Cai, Z. Zhang, Z. Yang, Z. Fang, S. Chen, X. Zhang, W. Li, Y. Zhang, H. Zhang, Z. Sun, Y. Zhang, Y. Li, L. Liu, W. Zhang, X. Xue, Performance of a superamphiphobic self-cleaning passive subambient daytime radiative cooling coating on grain and oil storage structures, Heliyon 9 (2023) e14599.
[36] Z. Yang, H. Zhang, Z. Zhang, M. Xian, Y. Shu, X. Gong, X. Cai, H. Jiang, Yuanzhu Cai, Z. Sun, Y. Zhang, Y. Li, W. Zhang, X. Xue, L. Liu, Sub-ambient daytime cooling effects and cooling energy efficiency of a passive sub-ambient daytime radiative cooling coating applied to telecommunication base stations— Part 1: distributed base stations and long-lasting self-cleaning properties, Energy 283 (2023) 128750.
[37] Y. Cai, Z. Yang, Z. Zhang, Z. Yang, H. Zhang, X. Xue, M. Xian, Y. Shu, X. Gong, X. Cai, H. Jiang, Y. Li, L. Liu, W. Zhang, Long-term cooling effects and cooling energy conservation of a subambient daytime radiative cooling coating relative to a cool-white coating over distributed telecommunication base stations, Sol. Energy 256 (2023) 127–139.
[38] N. Wang, Y. Lv, D. Zhao, W. Zhao, J. Xu, R. Yang, Performance evaluation of radiative cooling for commercial-scale warehouse, Mater. Today Eng 24 (2022) 100927.
[39] W. Xu, S. Gong, N. Wang, W. Zhao, H. Yin, R. Yang, X. Yin, G. Tan, Temperature reduction and energy-saving analysis in grain storage: field application of radiative cooling technology to grain storage warehouse, Renew. Energy 218 (2023) 119272.
[40] W. Xu, J. Tu, N. Xu, Z. Liu, Predicting daily heating energy consumption in residential buildings through integration of random forest model and meta-heuristic algorithms, Energy 301 (2024) 131726.
[41] M. Laskar, R. Masi, S. Karatasou, M. Santamouris, M. Assimakopoulos, On the impact of user behaviour on heating energy consumption and indoor temperature in residential buildings, Energy Build. 225 (2022) 111657.
[42] M. Santamouris, A. Synnefa, T. Karlessi, Using advanced cool materials in the urban built environment to mitigate heat islands and improve thermal comfort conditions, Sol. Energy 85 (2011) 3085–3102.
[43] E. Rephaeli, A.P. Raman, S. Fan, Ultrabroadband photonic structures to achieve high-performance daytime radiative cooling, Nano Lett. 13 (2013) 1457–1461.